nature communications

Article

https://doi.org/10.1038/s41467-026-74644-2

Spatiotemporal flux breathing and topological sculpting in structured transverse orbital angular momentum lattices

Received: 14 December 2025

Accepted: 4 June 2026

Published online: 24 June 2026

Check for updates

Dawei Liu[1,10], Xingyuan Zhang[2,10], Yonghang Tai[3,10], Daijun Luo[1], Huiming Wang[4], Zhirong Tao[5], Dana JiaShaner[1], Zhensheng Tao[6], Xiaoshi Zhang[7], Zhigang Peng[8], Guangyu Fan[1,3] & Qiwen Zhan[1,2,9]

Spatiotemporal optical vortices (STOVs) carrying transverse orbital angular momentum (OAM) fundamentally expand light-structuring capabilities. However, current rigid-body generation paradigms constrain transverse OAM to a single scalar property, leaving rich internal wavepacket dynamics inaccessible. This rigidity contrasts with ubiquitous natural vortices where symmetry breaking is the norm. Here, we break rotational symmetry via the nonlinear mapping of the azimuthal phase gradient, realizing programmable spatiotemporal flux breathing. We theoretically and experimentally demonstrate that local phase gradient variations induce instantaneous group velocity anisotropy. This compels local OAM density to spontaneously reorganize into stable, multilobed lattice structures while strictly preserving global topological charge. Furthermore, we harness these structures' modulation frequency for free-space information transfer, achieving high-fidelity encoding and decoding of spatiotemporal topological states. This work transitions STOVs from passive scalar objects to structured functional carriers, opening avenues for high-dimensional optical communications, ultrafast spatiotemporal manipulation, strong-field physics, and high-dimensional quantum entanglement.

Since the seminal recognition of orbital angular momentum (OAM) by Allen et al. in 1992[1], structuring light has evolved into a sophisticated discipline[2,3]. Over the past three decades, spatial OAM has blossomed into a rich ecosystem of structured fields, ranging from cylindrically symmetric modes to complex vector vortices and topological textures on the higher-order Poincaré sphere[4–6]. In stark contrast to these mature spatial modalities, the spatiotemporal optical vortex (STOV) represents a relatively nascent frontier[7,8]. First theoretically envisioned

[1]School of Optical-Electrical and Computer Engineering, University of Shanghai for Science and Technology, Shanghai, China. [2]Zhejiang Key Laboratory of 3D Micro/Nano Fabrication and Characterization, Department of Electronic and Information Engineering, School of Engineering, Westlake University, Hangzhou, Zhejiang, China. [3]Department of Physics and Electronic, Yunnan Normal University, Kunming, Yunnan, China. [4]Institute of Photonics, TU Wien, Vienna, Austria. [5]Karlsruhe Institute of Technology, Karlsruhe, Germany. [6]State Key Laboratory of Surface Physics and Department of Physics, Fudan University, Shanghai, China. [7]Yunnan University, Kunming, Yunnan, China. [8]Beijing Engineering Research Center of Laser Applied Technology, Beijing University of Technology, Beijing, China. [9]International Institute for Sustainability with Knotted Chiral Meta Matter (WPI-SKCM2), Hiroshima University, Higashihiroshima, Hiroshima, Japan. [10]These authors contributed equally: Dawei Liu, Xingyuan Zhang, Yonghang Tai. e-mail: gfan@usst.edu.cn

as electromagnetic flying doughnuts[9,10] and experimentally realized in 2016[11], STOVs have unlocked a unique transverse degree of freedom by embedding phase singularities into the ultrafast spatiotemporal domain ($x - t$)[12–14]. While this toroidal topology has bridged the gap between structured light and ultrafast optics[15,16], the field remains in its infancy regarding structural control. Current paradigms predominantly focus on the generation and conservation of the global topological charge, typically yielding isotropic, rigid-body wave packets[17,18]. Consequently, the transverse OAM is effectively treated as a monolithic scalar property, leaving the intricate local structural dynamics of the local phase space structure largely unexplored and unexploited.

Despite the rapidly growing interest in these electromagnetic toroids, current generation paradigms remain largely restricted to the rigid body regime. Standard STOVs, whether generated through nonlinear collapse[11,18,19] or linear pulse shaping[7,17], are typically constructed using uniform spiral phases. This approach imposes a strict rotational symmetry akin to a solid flywheel in which the azimuthal phase velocity remains invariant. Consequently, the resulting wave packets manifest as isotropic, featureless doughnut-like wave packets characterized by an angular momentum density that is evenly distributed along the ring[16]. While mathematically elegant, this symmetry conceals a fundamental physical limitation by treating the optical vortex as an incompressible rigid object rather than a dynamic fluid. Yet, in ubiquitous natural vortex systems ranging from quantum fluids to atmospheric cyclones, non-uniform rotation and symmetry breaking are the norm rather than the exception[20–23]. In such fluid-like regimes, the continuity of flux dictates a profound link between motion and structure, where local deceleration of the flow compels matter to accumulate into high-density lobes while acceleration leads to rarefaction. Within the optical regime, the breaking of this rigid rotational symmetry has already yielded profound dynamics in the spatial domain, where non-canonical vortices with structured phase gradients exhibit accelerated rotation and fluid-like energy redistribution[24]. Concurrently, recent advancements in temporal phase manipulation have begun to unlock complex subcycle spatiotemporal modulations[25]. The inability to break the rotational symmetry of STOVs has thus historically prevented access to this fluid-like dynamics of structured spatiotemporal wavepackets, effectively locking the potential for internal energy sculpting behind a rigid phase constraint.

In this work, we show that spatiotemporal optical vortices can be structured beyond the rigid-body regime by sculpting their local azimuthal phase gradients while preserving the global phase winding. We experimentally realize non-uniform spatiotemporal optical vortices through a nonlinear mapping of the spectral azimuthal phase, which converts a rotationally symmetric STOV into a programmable spatiotemporal lattice. In this framework, the modulation depth sets the degree of local anisotropy and the modulation frequency sets the number of lattice lobes, providing direct control over the internal structure of the wave packet. The resulting fields exhibit spatiotemporal flux breathing, in which the transverse energy flow and angular-momentum density periodically expand and compress along the azimuthal coordinate. Simulations and measurements show that this local redistribution is deterministic and remains compatible with conservation of the global topological charge[17,26,27]. We further demonstrate that the modulation frequency and topological charge form two independent indices for free-space information encoding, allowing high-fidelity decoding of spatiotemporal topological symbols. Our results provide a route to controlling the topology, dynamics and information content of ultrafast structured light.

Results

Theoretical analysis

To establish a comprehensive physical framework for the Non-uniform Spatiotemporal Optical Vortex (NSTOV), we explicitly examine the field formation within the spectral domain (k_x, ω). Conventional generation paradigms impose a linear helical phase dependence $\Phi(\theta) = \ell\theta$, which strictly enforces an isotropic ring geometry due to the inherent rotational symmetry of the Fourier transform. To transcend this geometric rigidity, we introduce a generalized azimuthal mapping function $f(\theta)$ for the spectral azimuthal coordinate θ, yielding the spectral field expression:

$$E(k_x, \omega) = A(k_x, \omega)\exp[-i\ell f(\theta)], \tag{1}$$

where $A(k_x, \omega)$ denotes the spectral envelope. Here, $f(\theta)$ represents an arbitrary smooth function subject to two rigorous topological boundary conditions. The first is the value-matching condition $f(\theta + 2\pi) - f(\theta) = 2\pi$, which imposes a strict quantization on the spectral phase winding to ensure that the global topological charge ℓ remains conserved. The second is the continuous derivative condition $f'(\theta + 2\pi) = f'(\theta)$, which guarantees a smooth phase gradient across the azimuthal boundary. This derivative constraint is physically essential, as a discontinuous phase gradient would unphysically scatter light and create arbitrary line singularities in the spatiotemporal energy flow.

To systematically engineer such structured lattices, we implement a harmonic perturbation model defined by the mapping function $f(\theta) = \theta + \alpha\sin(m\theta)$, as visualized in the phase waveforms and maps of Fig. 1a, b. In this regime, the spatiotemporal geometry is governed by two dimensionless control parameters: the modulation depth α, which determines the magnitude of anisotropy, and the modulation frequency m, which dictates the rotational symmetry order of the resulting lattice (see Supplementary Note 1). The physical driver of the spatiotemporal reconstruction is the non-uniformity of the spectral phase gradient:

$$\frac{\partial\Phi}{\partial\theta} = \ell[1 + \alpha m\cos(m\theta)]. \tag{2}$$

This local gradient represents the azimuthal mapping rate from the spectral to the spatiotemporal domain. The cosine modulation implies that the mapping velocity oscillates periodically, creating alternating sectors of spectral expansion (associated with high gradients) and compression (associated with low gradients), thereby setting the stage for the deterministic redistribution of energy. Furthermore, the sign of the modulation depth α strictly dictates the spatial orientation of the energy redistribution. A negative α ($\alpha < 0$) physically inverts the azimuthal phase modulation. This means the regions of angular acceleration and deceleration are spatially flipped by an angle of π/m radians relative to the positive α regime. We illustrate this symmetric correspondence in the updated conceptual diagram of Fig. 1, which now explicitly compares the morphological transformations for both $\alpha > 0$ and $\alpha < 0$ to provide an intuitive baseline for our generalized framework.

The transformation from this spectral modulation to the physical spatiotemporal intensity distribution is elucidated via the stationary phase approximation. The local intensity I_{ST} is asymptotically governed not by the gradient itself, but by the variation of the gradient—specifically, the spectral phase curvature. The photon flux density scales inversely with the magnitude of the second derivative of the spectral phase:

$$I_{ST} \propto \left|\frac{d^2\Phi}{d\theta^2}\right|^{-1} \approx \frac{1}{|\ell\alpha m^2\sin(m\theta)|}. \tag{3}$$

This divergence unveils a deterministic transport mechanism: energy is effectively depleted from regions exhibiting high curvature—where the local phase gradient varies rapidly—and coalesces within sectors characterized by stationary phase gradients (vanishing curvature). This geometric accumulation forms spatiotemporal spectral caustics,

 https://doi.org/10.1038/s41467-026-74644-2

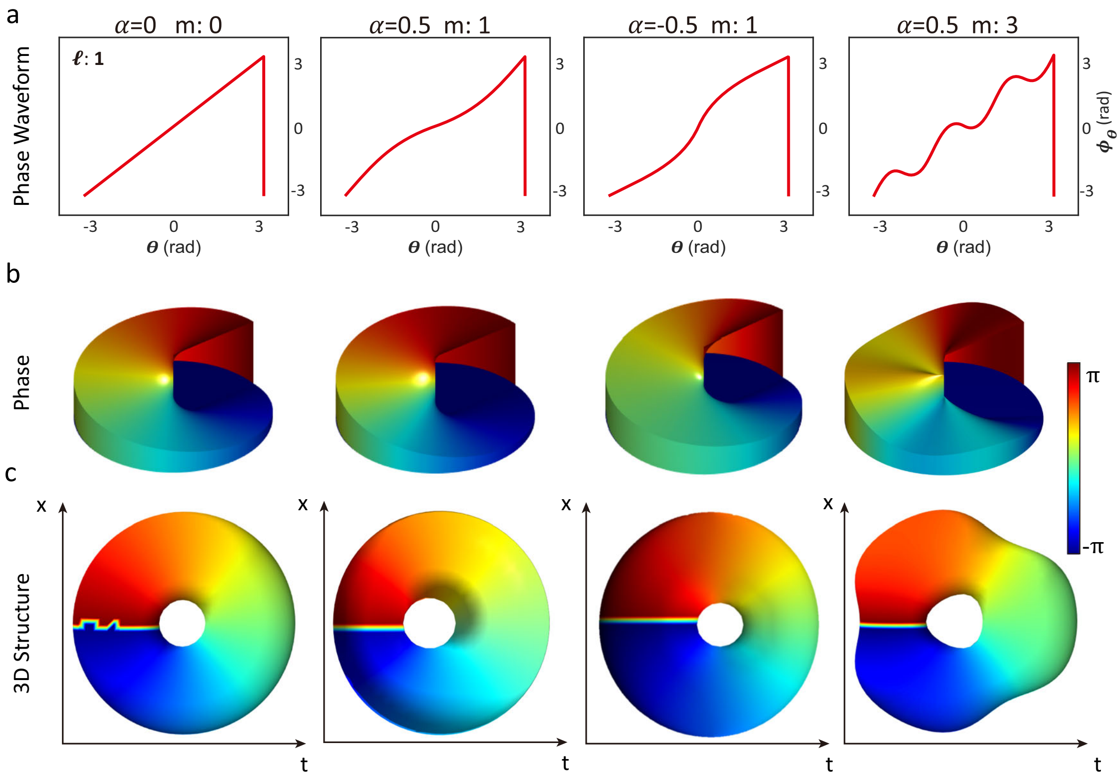

Fig. 1 | Non-uniform phase mapping and the corresponding three-dimensional temporal structure of the NSTOV. a Phase variation profiles under different degrees of non-uniform manipulation. **b** Phase maps corresponding to different manipulation parameters. **c** Schematic illustration of the three-dimensional spatiotemporal structure of the NSTOV generated under various non-uniform phase manipulations.

which serve as the structural skeleton for the bright lobes. Although physical diffraction effects smooth these mathematical singularities into finite intensity peaks—a process rigorously described by the multimode interference model in Supplementary Note. In the context of Catastrophe Theory, the formation of the NSTOV lattice corresponds to a fold catastrophe, where the photon flux is geometrically focused onto specific stable spatiotemporal trajectories. Consequently, the modulation parameters α and m function as deterministic control variables that manipulate the topology of the caustic surface.

Crucially, this drastic local structural reconfiguration proceeds under a strict global topological constraint. The spectral mapping function adheres to the rigorous boundary condition $f(\theta + 2\pi) - f(\theta) = 2\pi$, which imposes a quantization restriction on the spectral phase winding. This boundary condition ensures that the closed-loop contour integral of the phase gradient in the spatiotemporal domain—which defines the physical topological charge—remains invariant:

$$\frac{1}{2\pi}\oint_C \nabla\Phi \cdot d\mathbf{l} = \ell. \tag{4}$$

This invariance implies that the NSTOV and the standard uniform STOV belong to the same homotopy class; despite their distinct intensity morphographies, they are topologically equivalent and can be smoothly transformed into one another via continuous deformation. To quantitatively characterize this symmetry-breaking transition, we define the lattice contrast parameter C as an effective order parameter:

$$C = \frac{I_{max} - I_{min}}{I_{max} + I_{min}}. \tag{5}$$

This parameter scales monotonically with the modulation depth α, confirming that the system undergoes a continuous evolution from a fluid-like uniform ring (possessing continuous $U(1)$ symmetry) to a highly crystallized rigid lattice structure (reduced to discrete C_m symmetry). This transition is governed by the deterministic interplay between local geometric sculpting—driven by the spectral phase curvature—and rigorous global topological protection.

Evolution from isotropic rings to spatiotemporal lattices

The transition from a uniform STOV to an NSTOV represents a fundamental symmetry-breaking event in the spatiotemporal domain. Figure 2a captures this morphological evolution for a fixed modulation frequency $m = 1$ as the modulation depth α is tuned from negative to positive values. As rotational symmetry is broken, the intensity distribution transforms from a featureless annulus into a structured lattice. Notably, the sign of α dictates the spatial orientation of the wave packet: switching from negative to positive α results in a spatiotemporal inversion of both the intensity lobes and the phase structures along the azimuthal coordinate. This manifestation confirms that the sign of the modulation directly controls the angular positioning of the structural features. In the limit of $\alpha = 0$, the field reverts to the isotropic geometry of a STOV, confirming that the emergence of these localized nodes originates entirely from the prescribed azimuthal nonlinearity.

To elucidate the microscopic mechanism of this transformation, we correlate the spatiotemporal intensity variation with the reconstructed phase topology in Fig. 2b. The measured phase profile exhibits periodic oscillations in its slope, delineating alternating sectors of angular "acceleration" and "deceleration." Physically, this non-uniform phase gradient constitutes a tailored kinematic landscape that reshapes the local group velocity of the wave packet. To systematically quantify this mechanism, Fig. 2c presents a theoretical 3D mapping of

https://doi.org/10.1038/s41467-026-74644-2

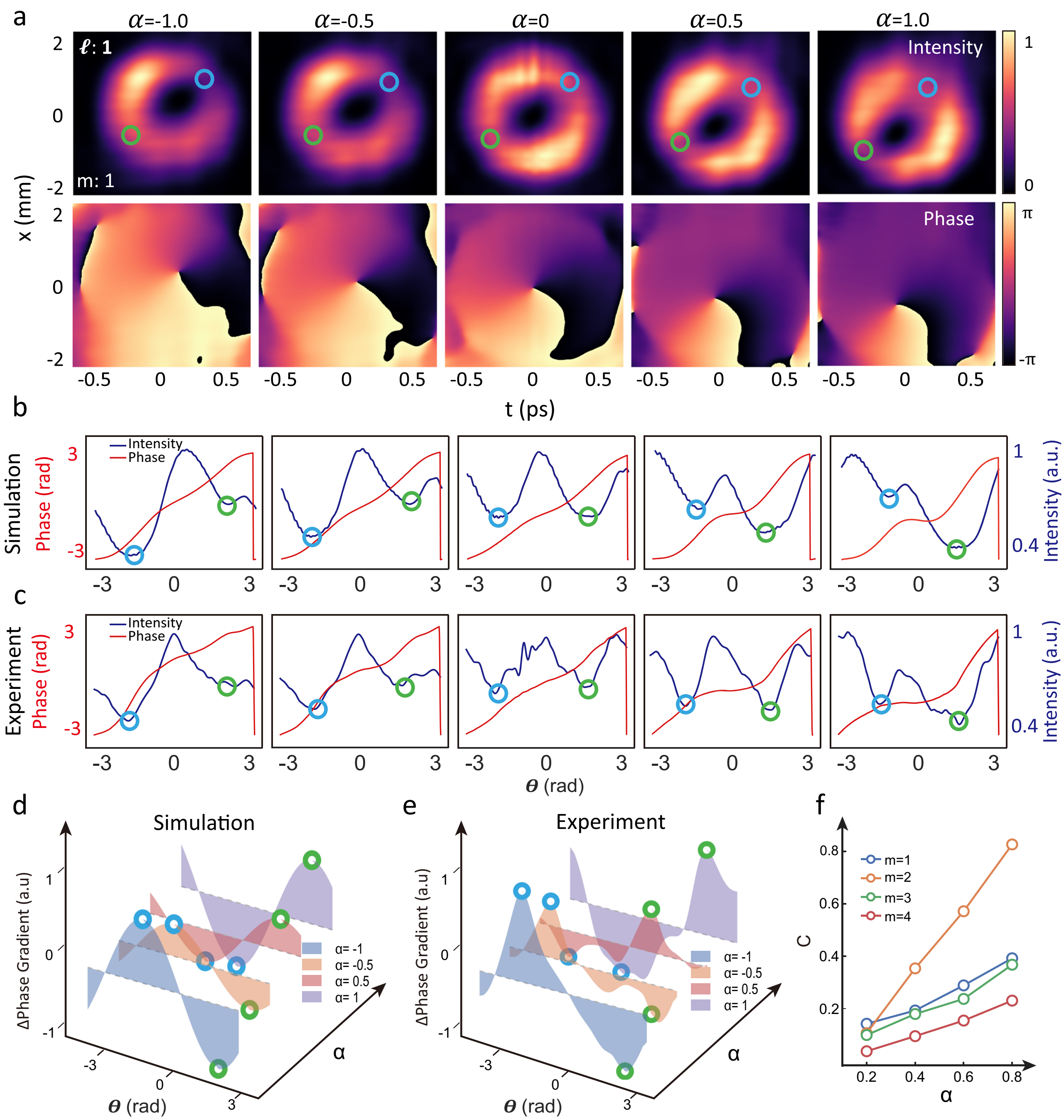

Fig. 2 | Temporal profiles and phase evolution of NSTOVs under different degrees of non-uniform phase manipulation. **a** Experimental intensity (top) and phase (bottom) for $\alpha \in \{-1.0, -0.5, 0, 0.5, 1.0\}$ at $m = 1$, revealing a spatiotemporal inversion upon reversing the sign of α. **b** Azimuthal traces of intensity and phase extracted along the NSTOV ring. **c** Theoretical phase gradient $\partial_\theta \Phi(\theta, \alpha)$, where the sign of α transposes kinematic zones and its magnitude $|\alpha|$ governs the gradient amplitude and velocity transition steepness. **d** Simulated phase gradient $\partial_\theta \Phi(\theta, \alpha)$. **e** Experimentally reconstructed phase gradient $\partial_\theta \Phi(\theta, \alpha)$. **f** Lattice contrast C as a function of $|\alpha|$, quantifying the transition from isotropic to structured lattices for various m.

the azimuthal phase gradient $\partial_\theta \Phi$ as a function of θ and α. This analysis reveals that α serves as a symmetry-inversion parameter: a sign reversal in α transposes the positions of the gradient maxima and minima, driving the observed spatial inversion. Furthermore, the magnitude $|\alpha|$ governs the modulation depth, where higher values increase the steepness of the local velocity transitions. The simulated and experimentally reconstructed phase gradients are presented in Fig. 2d, e respectively. The high-fidelity agreement between the experimental reconstruction and the numerical model verifies the phase-gradient landscape as the deterministic driver for the observed spatiotemporal reconstruction. Finally, the extent of this symmetry breaking is quantified via the lattice contrast C in Fig. 2f. The monotonic scaling of C with $|\alpha|$ across various m underscores a continuous transition from an isotropic annulus ($C \approx 0$) toward a discrete, high-contrast lattice configuration, establishing α as the effective order parameter governing the spatiotemporal morphology.

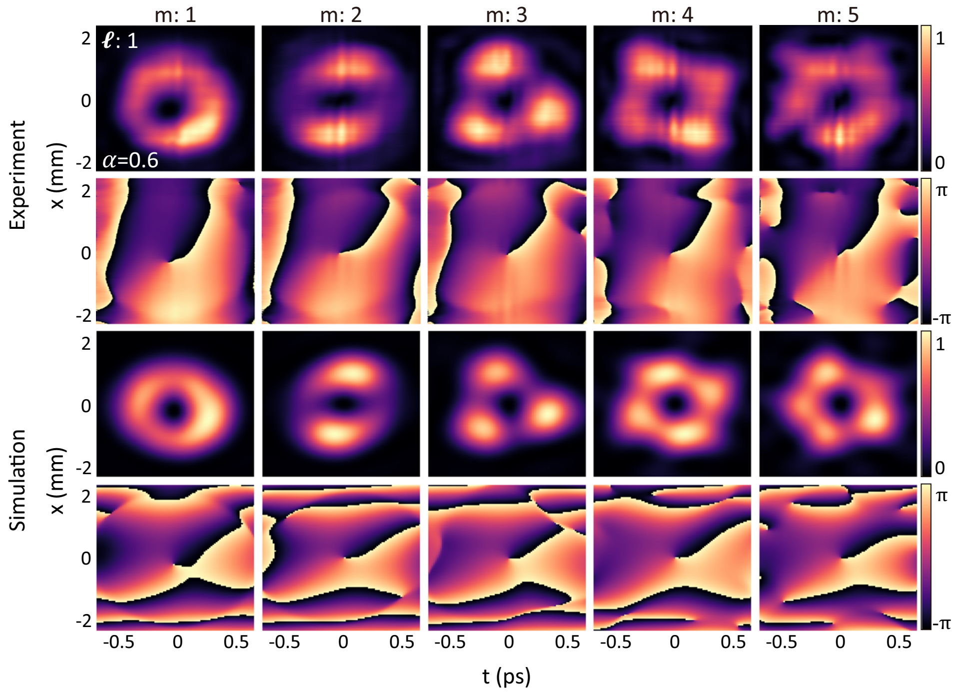

Fig. 3 | Experimental and simulated comparison of NSTOVs generated with different azimuthal manipulation frequencies *m* at a fixed manipulation amplitude *α*. Temporal intensity and phase distributions exhibit multiple bright sectors whose number corresponds to the value of *m*.

Global topological protection and discrete symmetry breaking

The NSTOV embodies a fundamental duality defined by the coexistence of drastic local structural reconfiguration and strict global topological integrity. Although the azimuthal phase profile undergoes severe distortion due to the non-uniform mapping, the function rigorously adheres to the boundary condition $f(\theta + 2\pi) - f(\theta) = 2\pi$. This quantization constraint ensures that the total phase accumulation along any closed loop enclosing the singularity remains invariant at $2\pi\ell$. Consequently, the global topological order of the field is robustly protected even as the azimuthal distribution of the phase gradient and angular momentum density is locally reshaped into complex geometries.

Figure 3 captures the emergence of these structured states by illustrating the evolution of the intensity distribution for a fixed modulation depth $\alpha = 0.6$ as the azimuthal modulation frequency m varies. The field transitions from a single asymmetric lobe at $m = 1$ to highly structured lattices exhibiting discrete rotational symmetries. For the $m = 2$ case, two localized energy nodes appear at antipodal positions to display a clear dipole-like structure. As the frequency increases to $m = 3$, the field evolves into a triangular lattice with three evenly spaced lobes and subsequently progresses to a five-fold symmetric arrangement of bright spots for $m = 5$. The number of generated lobes is strictly determined by the modulation frequency m, with the intensity maxima spatially coinciding with the extrema of the phase perturbation $\sin(m\theta)$. This deterministic mapping confirms that the azimuthal intensity landscape is a direct physical manifestation of the periodic phase gradient. Crucially, despite the formation of these discrete islands of high intensity, the net phase winding over the full rotation remains topologically quantized at $2\pi\ell$, verifying the conservation of the system's global topological charge.

This interplay between local symmetry breaking and global conservation reveals the intrinsic topological robustness of the NSTOV. Within specific angular sectors, the local phase wavefronts are elastically stretched or compressed to effectively redistribute the energy flux without severing the phase singularity. This mechanism is analogous to the principle of local asymmetry with global invariance found in condensed matter physics, much like how local wavefunctions in a topological insulator may deform under perturbations while the global Chern number remains fixed. The NSTOV thus serves as a tangible optical analogue that visualizes how robust global topological invariants can coexist with—and indeed govern—rich local dynamical diversities within a single spatiotemporal field.

Energy flow and spatiotemporal flux breathing

Beyond the static intensity profile, a defining signature of the NSTOV is the dynamic reconstruction of its energy flow and angular momentum. In the context of singular optics, the instantaneous direction of energy transport is dictated by the local Poynting vector, $\mathbf{S} \propto \mathrm{Im}(E^{*}\nabla E)$, whose azimuthal component S_θ is directly proportional to the phase gradient $\partial_\theta \Phi$. For the NSTOV, this gradient follows the modulation $\partial_\theta \Phi = \ell[1 + \alpha m \cos(m\theta)]$, implying that the local phase curvature acts as a throttle for energy circulation: regions of high gradient manifest as accelerated sectors with enhanced transverse momentum density, whereas low-gradient regions behave as decelerated zones where energy flow is transiently retarded.

This periodic variation establishes a dynamic equilibrium governed by global conservation, manifesting as a phenomenon we term spatiotemporal flux breathing. To explicitly reveal the underlying optical field structure driving this dynamics, we decompose the spatiotemporal profiles of intensity, phase, and phase gradient in Fig. 4. The experimental maps across varying modulation frequencies ($m = 1$ to 5) demonstrate a persistent anti-phase correlation: the localized intensity minima (dark regions) consistently coincide with the sharpest phase gradients ($|\nabla \varphi|$, Fig. 4k–o). Driven by this non-uniform structural landscape, the energy flow and angular momentum undergo a striking rhythmic reconstruction, as visualized in Fig. 5. The close correspondence between the numerical simulations (Fig. 5a–e) and experimental measurements (Fig. 5k–o) vividly illustrates that as energy is locally accelerated in one sector, it is compensated by deceleration in adjacent regions, creating a rhythmic oscillation of the azimuthal flux. A concomitant redistribution occurs for the angular

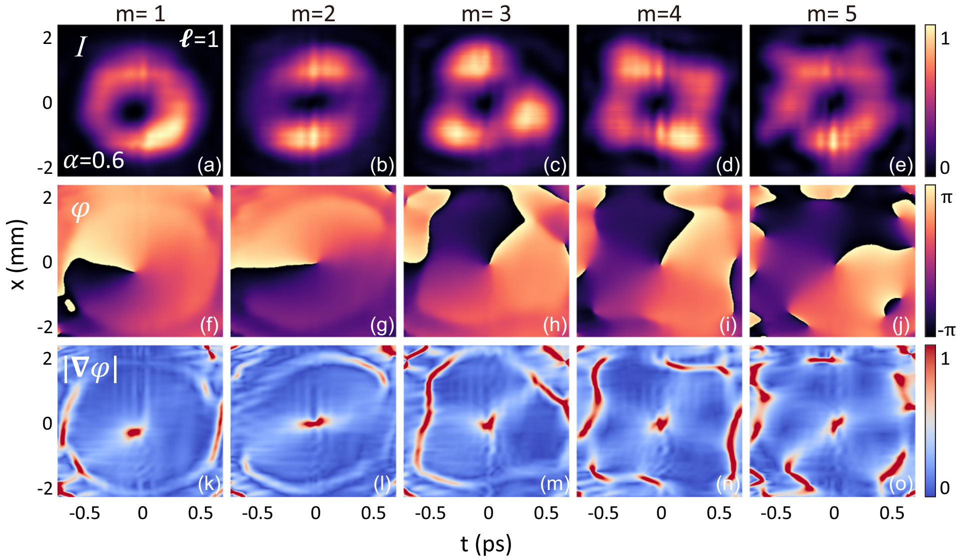

Fig. 4 | Spatiotemporal decomposition of intensity, phase, and phase gradient in NSTOVs. The columns correspond to increasing azimuthal modulation frequencies from $m = 1$ to $m = 5$ with a fixed topological charge $\ell = 1$. **a**–**e** Normalized spatiotemporal intensity distributions I. **f**–**j** Corresponding measured phase maps φ. **k**–**o** Magnitude of the reconstructed local phase gradient $|\nabla\varphi|$. A persistent anti-phase correlation is experimentally observed, where localized intensity minima (dark regions) consistently coincide with the maxima of the local phase gradient, confirming the gradient-driven spectral rarefaction mechanism.

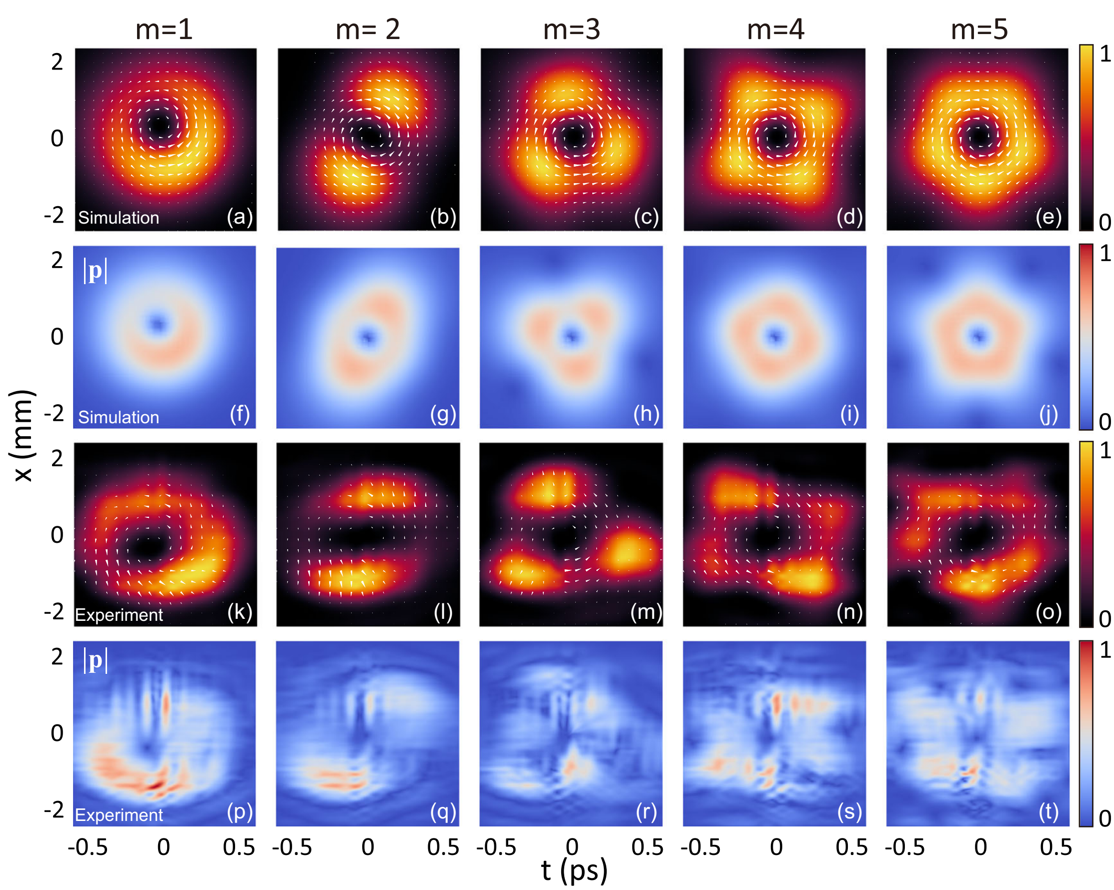

Fig. 5 | Visualization of spatiotemporal flux breathing and momentum density competition. The columns correspond to varying modulation frequencies from $m = 1$ to $m = 5$. **a**–**e** Simulated normalized intensity overlaid with transverse Poynting vector arrows, indicating the local direction and relative magnitude of energy flow. **f**–**j** Simulated magnitude of the momentum density $|\mathbf{p}|$. **k**–**o** Corresponding experimental intensity and energy flow vector maps. **p**–**t** Experimentally reconstructed momentum density magnitude $|\mathbf{p}|$. The results reveal a distinct structural transition driven by the competitive interplay between local photon density and phase velocity: for $m \leq 2$, the momentum density maxima coincide with the high-intensity lobes, whereas for $m \geq 3$, the dominant steep phase variations shift the momentum maxima entirely into the low-intensity regions.

momentum density, $L_z = rS_\theta$, which oscillates reciprocally between neighboring sectors. These results confirm that this transport is strictly conservative: while the local distribution of angular momentum undergoes drastic periodic rearrangement, the total angular momentum—calculated as the ensemble average $\langle L_z \rangle_{\text{total}} = (1/2\pi)\int_0^{2\pi} L_z(\theta)\, d\theta$—remains invariant throughout the evolution.

The azimuthal momentum density distribution $p_\theta(\theta)$ is governed by the competitive interplay between the local photon density and the instantaneous phase velocity, expressed as:

$$p_\theta(\theta) \propto I(\theta)\frac{\partial \Phi}{\partial \theta} \propto I(\theta) \cdot \ell[1 + \alpha m \cos(m\theta)]. \tag{6}$$

Since the spatiotemporal flux breathing mechanism dictates that intensity $I(\theta)$ accumulates in regions of local deceleration (where the phase gradient $\partial_\theta \Phi$ is minimal), these two terms in Eq. (6) are intrinsically inversely correlated, as proven by the structural decomposition in Fig. 4. For the regime of lower modulation frequencies ($m \le 2$), the drastic accumulation of local intensity $I(\theta)$ dominates the slight reduction in phase gradient, resulting in a momentum density distribution that remains in-phase with the intensity profile. Conversely, in the higher frequency regime ($m \ge 3$), the modulation factor αm becomes significant, causing the local phase gradient to approach zero at the intensity maxima. This severe suppression of the local phase velocity overrides the contribution of photon concentration, leading to a local minimum in the momentum density and an effective anti-phase relationship between intensity and momentum. This regime-dependent behavior finds quantitative support in the structural parameter C presented in Fig. 2f, which characterizes the relative weight of the non-uniform field component and varies non-monotonically with modulation order m. At $m = 2$, C reaches its maximum, such that the photon-density-driven term overwhelmingly governs the momentum distribution and p_θ closely tracks the intensity profile. For $m > 2$, the progressively growing amplitude of the phase gradient with increasing m renders phase topology the dominant factor over local photon density. Notably, although the C value at $m = 1$ is comparable to that at $m = 3$, the substantially smaller phase gradient amplitude at $m = 1$ ensures that the momentum density remains intensity-governed, consistently placing it within the low-m regime. We visualize the ultimate outcome of this competitive mechanism through the simulated and experimental momentum density maps ($|\mathbf{p}|$) in Fig. 5f–j and Fig. 5p–t. Crucially, the influence of the phase gradient term scales with the modulation order m: while the momentum distribution is dominated by the photon density at low topological charges, the steep phase variations characteristic of higher-order singularities increasingly govern the local energy flow. For $m \ge 3$, this gradient-driven contribution compensates for the vanishing photon density in the dark regions, resulting in a distinct migration of momentum maxima from the bright lobes toward the intensity nulls. Further discussion regarding this phenomenon is provided in Supplementary 2.

From a broader physical perspective, this coupled evolution of energy flow and phase topology constitutes an optical analogue of a topological pump. The azimuthal coordinate θ serves as a cyclic parameter space, where the non-uniform mapping $f(\theta)$ drives the adiabatic-like transfer of the topological quantity (angular momentum) between local sectors. Accelerated regions effectively emit angular momentum flux while decelerated regions absorb it, all within a globally conserved system. Unlike discrete topological pumps in condensed matter lattices, the NSTOV offers a continuous, directly visualizable platform where the interplay between topological structure and dynamical flow can be explored, providing a new paradigm for unifying topology and energetics in ultrafast light fields.

Multidimensional information encoding with NSTOV

The intrinsic duality of the NSTOV, characterized by the coexistence of global topological conservation and local structural reconfiguration, naturally lends itself to high-dimensional information encoding. By harnessing the distinct spatiotemporal morphologies derived from our theory, we establish a dual-domain encoding protocol that spans both topological and structural degrees of freedom. Specifically, the modulation frequency m discretizes the wave packet into a lattice with m-fold rotational symmetry that determines the number of lobes, while the topological charge ℓ dictates the global helical winding of the phase. Crucially, these two degrees of freedom are physically orthogonal, meaning that the local intensity distribution determined by m does not perturb the net phase accumulation defined by ℓ, and vice versa. This independence provides two decoupled axes for data modulation, allowing us to treat each NSTOV pulse as a two-dimensional symbol $S_j = (\ell_j, m_j)$ within a joint encoding space.

To validate this capability, we implemented a high-dimensional coding scheme using a parameter space defined by $\ell \in \{-3, -2, -1, 1, 2, 3\}$ and $m \in \{0, 1, 2, 3, 4\}$. As illustrated in Fig. 6a, mapping these states onto binary values enables a single NSTOV pulse to carry an information entropy of approximately 4.9bits. To further scale the transmission capacity, we synthesized temporal arrays of NSTOV pulses (NSTOVAs) as depicted in Fig. 6b. Using coherent detection, we retrieve the full spectral amplitude and phase of the pulse train (Fig. 6c), from which the time-domain intensity and phase profiles are reconstructed via spectro-temporal transformation.

As a proof-of-concept validation, we synthesized two NSTOV arrays, each consisting of a temporal sequence of three sub-pulses encoding the symbol vectors (ℓ, m) = [(1, 3), (2, 2), (3, 1)] and [(−1, 3), (−2, 2), (−3, 1)], respectively. Collectively, these sequences constitute a dense data packet with an information capacity of approximately 14bits. Benefiting from the mutual orthogonality between the structural periodicity and the topological helicity, the receiver can demultiplex the ℓ and m indices for each time slot with negligible crosstalk. Exploiting this robust recoverability, we successfully transmitted and reconstructed a 28-bit image of the emblem of the University of Shanghai for Science and Technology (Fig. 6d). To quantify this advantage, the information capacity per pulse is calculated as $C = \log_2(N_l \times N_m)$. Using 6 topological ($N_l$) and 5 structural ($N_m$) states, an NSTOV pulse carries approximately 4.9 bits. In contrast, conventional STOVs ($m = 0$) are restricted to a single coding axis, yielding only $\log_2(6) \approx 2.58$ bits per pulse. Consequently, our 3-pulse NSTOVA sequence achieves 14.7 bits, nearly doubling the 7.7 bits of a conventional STOV array. Practically, transmitting the 28-bit logo (Fig. 6d) requires only 6 NSTOV sub-pulses, whereas conventional STOVs would necessitate 11. Notably, we also found that this flux breathing property can be preserved during frequency conversion, for example in second harmonic generation (See Supplementary 3). This demonstration verifies that the phenomena of spatiotemporal flux breathing and topological protection can be effectively harnessed to establish a practical, high-dimensional alphabet for optical information processing.

Discussion

The realization of the non-uniform spatiotemporal optical vortex represents a paradigm shift in the structuring of light, transitioning from the generation of passive, isotropic phase singularities to the active sculpting of spatiotemporal topology. By breaking the rotational symmetry of the phase, we unlock a regime of spatiotemporal flux breathing, where the energy flow and angular momentum density undergo deterministic, periodic reconstruction. This mechanism reveals a fundamental duality: the local field topology is elastic and reconfigurable, yet it is rigidly anchored by the global topological invariant. Unlike conventional STOVs that behave as rigid bodies[7], the

https://doi.org/10.1038/s41467-026-74644-2

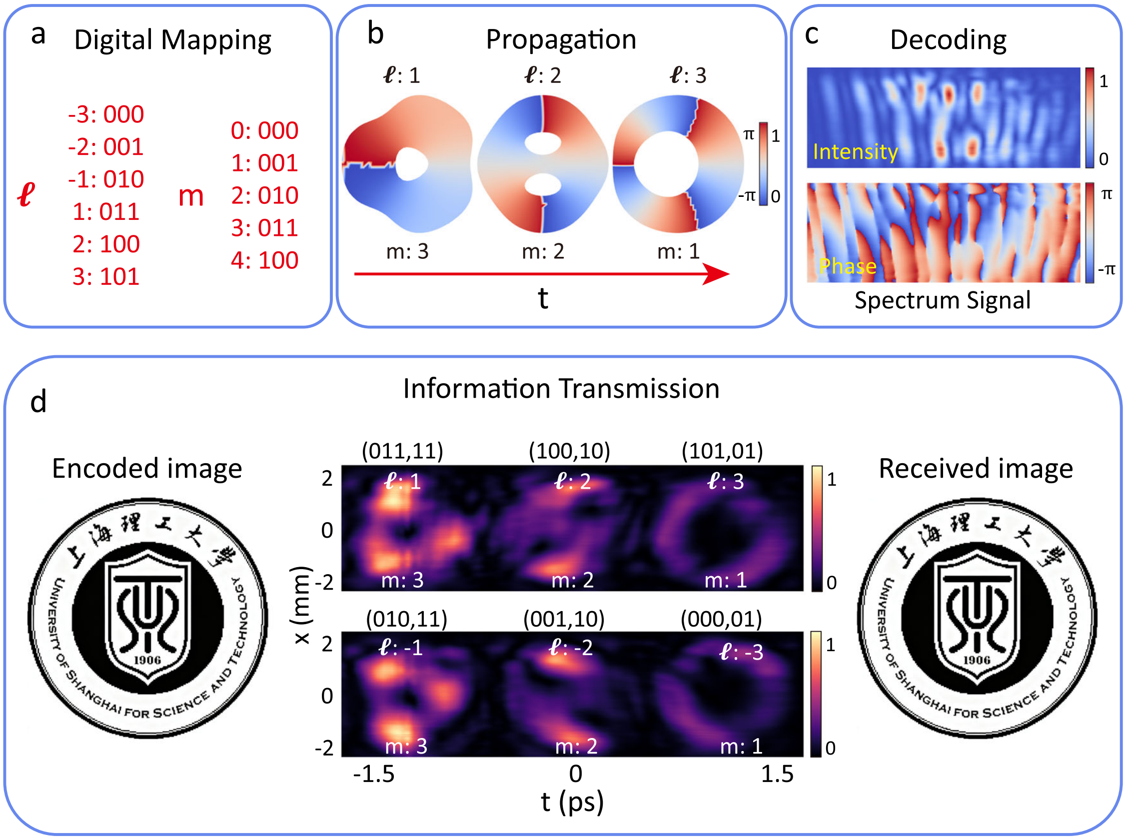

Fig. 6 | Multidimensional information encoding and transmission using NSTOV. a Digital encoding scheme in which the topological charge ℓ and the non-uniform manipulation frequency m are individually mapped onto binary strings, forming a two-dimensional symbol space. **b** Transmission of the NSTOV pulses carrying the encoded information. **c** Retrieved spectral amplitude and phase of the NSTOVA at the receiver, obtained through coherent detection followed by spectro-temporal reconstruction. **d** Demonstration of high-dimensional optical communication: two NSTOVAs enable the successful transmission of a 28-bit logo image, confirming the practical feasibility of NSTOV-based multidomain encoding.

NSTOV functions as a dynamic lattice, allowing for the precise lithography of ultrafast wave packets in the continuous spatiotemporal domain. Experimentally, we have confirmed that the azimuthal modulation frequency m serves as a robust control knob for determining the symmetry of the energy flow. The successful translation of this physical orthogonality into a multidimensional information encoding protocol validates the NSTOV as a functional information carrier. By mapping the structural degree of freedom (lattice symmetry) and the topological degree of freedom (winding number) onto independent coding axes, we establish a high-density alphabet resilient to intermodal crosstalk. This goes beyond simple multiplexing; it implies that the internal geometry of a spatiotemporal singularity can be treated as a programmable logic unit for optical processing.

Looking ahead, the structural versatility of our framework extends far beyond the analytical elegance of the harmonic mapping $f(\theta)=\theta+\alpha\sin(m\theta)$. Because the methodology is fundamentally universal, incorporating higher-order Fourier harmonics into $f(\theta)$ enables the inverse-design of arbitrary lattice structures that feature non-uniform petal spacing, varying lobe intensities, and asymmetric substructures, provided the continuous derivative boundary condition, $f'(\theta+2\pi)=f'(\theta)$, is satisfied to ensure a physically smooth wavepacket. Realizing increasingly complex spatiotemporal topologies presents exciting frontiers in both generation and transmission. At the generation stage, synthesizing states with ultra-high l or m values necessitates rapid azimuthal phase wrapping. While currently bounded by the Nyquist limit of the spatial light modulator (SLM) pixel pitch, advancing SLM resolutions will naturally unlock these higher-dimensional states without spatial aliasing. Beyond generation, deploying NSTOVA sequences in complex, dispersive media (e.g., optical fibers or atmospheric turbulence) offers a compelling avenue for future research. While dispersion-induced temporal broadening may introduce inter-symbol interference (ISI) that affects the fine-grained structural index m, the global topological charge l inherently maintains strong topological protection against such localized perturbations. To fully preserve the joint state $S_j=(l_j, m_j)$ over long distances, this framework can seamlessly integrate established signal processing techniques, such as transmitter pre-chirping or deep-learning-based MIMO equalizers. Ultimately, these extensions pave the way for resilient, ultra-high-capacity spatiotemporal optical networks.

The NSTOV architecture provides a versatile platform that naturally connects to several emerging frontiers in physics. In the realm of strong-field physics and attosecond science, the controllable transverse OAM offers a precise mechanism for steering electron trajectories. Embedding these breathing vortices into high-intensity drivers could extend beyond the generation of time-varying OAM[18,28] to the creation of attosecond spatiotemporal lattices. Here, the non-uniform field modulation would be mapped onto the recolliding electrons, potentially yielding XUV pulse trains that inherit the multi-lobed lattice structure[14]. This offers a bold prediction for sculpting matter waves on atomic scales and temporal resolutions.

Furthermore, the principle of local asymmetry with global invariance links our work directly to topological photonics. The NSTOV can be conceptualized as a platform for optical synthetic dimensions, where the azimuthal coordinate θ serves as a periodic parameter space. By adiabatically modulating the breathing depth α or the propagation dynamics, one could realize topological pumping of energy between lattice sites, exploring edge-state dynamics and topological phase transitions in a continuous spatiotemporal medium rather than discrete arrays[29,30]. Finally, in the context of quantum information, the multidimensional nature of NSTOVs enables the pursuit of hyper-entanglement. Since the topological charge ℓ and the lattice symmetry order m constitute physically orthogonal degrees of freedom, photon pairs can be entangled simultaneously across both indices. This capability allows for the construction of ultra-high-dimensional Hilbert spaces, offering significant advantages for noise-resilient quantum communication and high-capacity Quantum Key Distribution (QKD)[31–33]. Collectively, these perspectives indicate that non-uniform spatiotemporal vortices are not merely a new class of structured beams, but a general instrument for engineering the topology, dynamics, and information content of light across the classical and quantum regimes.

Methods

Non-uniform phase generation

The synthesis of NSTOVs relies on the precise imposition of a structured phase mask within the spatiotemporal spectral domain. In our experimental 4f pulse-shaping setup, the spatial light modulator is positioned at the Fourier plane, where the disparate degrees of freedom of the light field are mapped onto the two-dimensional spatial coordinates of the modulator. Specifically, the diffraction grating disperses the temporal frequency components ω along the vertical axis of the SLM (y_{SLM}), while the cylindrical lens performs a Fourier transform in the transverse dimension, mapping the spatial frequency components k_x along the horizontal axis (x_{SLM}).

To generate the target wave packet, we first define the spectral azimuthal coordinate θ in the (k_x, ω) plane. For each pixel (u, v) on the SLM, the corresponding azimuthal angle is calculated as:

$$\theta(u,v)=\arctan\left(\frac{\omega(v)-\omega_0}{k_x(u)}\right), \quad (7)$$

where ω_0 represents the central angular frequency of the carrier wave. Unlike the generation of conventional rigid-body STOVs, which utilize a linear helical phase $\Phi = \ell\theta$, we implement a non-linear azimuthal mapping function to break the rotational symmetry. The specific phase pattern Φ_{SLM} loaded onto the modulator is governed by the mapping function $f(\theta)$, defined as:

$$\Phi_{SLM}(k_x,\omega)=\ell f(\theta)=\ell[\theta+\alpha\sin(m\theta)], \quad (8)$$

where ℓ denotes the topological charge determining the global phase winding. The terms inside the brackets introduce the deterministically controlled anisotropy: α represents the dimensionless modulation depth, which dictates the magnitude of the local phase distortion, and m is the modulation frequency, which determines the rotational symmetry order of the resulting spatiotemporal lattice.

Crucially, this phase modulation is not merely a geometric artifact but acts as a deterministic driver for energy redistribution. Instead of a temporal group delay, the structural dynamics are governed by the local azimuthal phase gradient within the spectral domain. The introduction of the sinusoidal perturbation term creates an azimuthally varying gradient profile:

$$k_\theta(\theta)=\frac{\partial\Phi}{\partial\theta}=\ell[1+\alpha m\cos(m\theta)]. \quad (9)$$

This non-uniform phase gradient implies that the mapping from the spectral coordinate (θ) to the physical spatiotemporal domain is nonlinear. The oscillating gradient induces local expansion and compression of the effective spectral density: regions with rapid phase variations induces spectral rarefaction (leading to depletion), while regions with stationary phase gradients induces spectral concentration, compelling the photon flux to accumulate. This gradient-driven redistribution mechanism is the direct physical origin of the spatiotemporal flux breathing phenomenon observed in the time domain.

Finally, to accommodate the operating range of the liquid-crystal SLM, the computed phase Φ_{SLM} is wrapped into the interval $[0, 2\pi]$ via a modulo operation. The resulting phase mask, characterized by its non-uniform, curved singularity lines (as shown in Fig. 1), is then mapped to the 8-bit grayscale levels of the SLM for experimental generation. This digital holography approach ensures that while the local intensity structure is drastically reconfigured into an m-lobed lattice, the global topological invariant defined by the boundary condition $f(\theta + 2\pi) - f(\theta) = 2\pi$ and the smoothness requirement $f'(\theta+2\pi)=f'(\theta)$ remain strictly preserved.

Experimental setup

Non-uniform spatiotemporal optical vortices (NSTOVs) were synthesized using a folded 4f spatiotemporal pulse-shaping platform. The driving source was a Yb-based femtosecond laser centered at 1030 nm, delivering a spectral bandwidth of 10 nm, a pulse duration of 300 fs (FWHM), a repetition rate of 1 kHz and an average power of 1 W. The beam was divided into two arms. In the shaping arm, a diffraction grating with 1200 lines/mm and a cylindrical lens of focal length f = 200 mm dispersed the pulse along the spatial and temporal degrees of freedom, forming a one-dimensional Fourier plane where a phase-only spatial light modulator was positioned. The SLM imposed the designed azimuth-dependent phase pattern onto the spatial-frequency components. After passing through the second half of the 4f line, this phase was coherently mapped into the temporal domain, generating a NSTOV at the output.

The second arm provided a transform-limited Gaussian reference pulse. The NSTOV and reference beams were recombined collinearly, and their spectral interferograms were recorded for phase retrieval. This configuration enabled continuous tuning of the parameters (ℓ, m) and allowed direct measurement of the temporal structure of the NSTOV, including the emergence of local bright sectors, redistribution of phase gradients and the angular-momentum breathing dynamics observed during evolution.

Data availability

The source data supporting the findings of this study, including the data underlying the main figures, have been deposited in Figshare under DOI 10.6084/m9.figshare.32315982. The deposited dataset includes reconstructed spatiotemporal intensity and phase distributions, azimuthal phase-gradient profiles, momentum-density data, information-encoding and decoding datasets, and source data used to generate the plots. Additional information required to interpret the data is provided in the manuscript and Supplementary Information.

References

1. Allen, L., Beijersbergen, M. W., Spreeuw, R. & Woerdman, J. Orbital angular momentum of light and the transformation of Laguerre-Gaussian laser modes. *Phys. Rev. A* **45**, 8185 (1992).
2. Molina-Terriza, G., Torres, J. P. & Torner, L. Twisted photons. *Nat. Phys.* **3**, 305–310 (2007).
3. Yao, A. M. & Padgett, M. J. Orbital angular momentum: origins, behavior and applications. *Adv. Opt. Photonics* **3**, 161–204 (2011).
4. Wang, J. et al. Terabit free-space data transmission employing orbital angular momentum multiplexing. *Nat. Photonics* **6**, 488–496 (2012).
5. Bozinovic, N. et al. Terabit-scale orbital angular momentum mode division multiplexing in fibers. *Science* **340**, 1545–1548 (2013).
6. Devlin, R. C., Ambrosio, A., Rubin, N. A., Mueller, J. B. & Capasso, F. Arbitrary spin-to-orbital angular momentum conversion of light. *Science* **358**, 896–901 (2017).

7. Chong, A., Wan, C., Chen, J. & Zhan, Q. Generation of spatio-temporal optical vortices with controllable transverse orbital angular momentum. *Nat. Photonics* **14**, 350–354 (2020).
8. Wan, C., Chong, A. & Zhan, Q. Optical spatiotemporal vortices. *Elight* **3**, 11 (2023).
9. Hellwarth, R. & Nouchi, P. Focused one-cycle electromagnetic pulses. *Phys. Rev. E* **54**, 889 (1996).
10. Papasimakis, N. et al. Pulse generation scheme for flying electromagnetic doughnuts. *Phys. Rev. B* **97**, 201409 (2018).
11. Jhajj, N. et al. Spatiotemporal optical vortices. *Phys. Rev. X* **6**, 031037 (2016).
12. Fang, Y., Lu, S. & Liu, Y. Controlling photon transverse orbital angular momentum in high harmonic generation. *Phys. Rev. Lett.* **127**, 273901 (2021).
13. Liu, Y. et al. Integrated vortex soliton microcombs. *Nat. Photonics* **18**, 632–637 (2024).
14. Martín-Hernández, R. et al. Extreme-ultraviolet spatiotemporal vortices via high harmonic generation. *Nat. Photonics* 19, 817–824 (2025).
15. Bliokh, K. Y. & Nori, F. Spatiotemporal vortex beams and angular momentum. *Phys. Rev. A- At. Mol. Opt. Phys.* **86**, 033824 (2012).
16. Wan, C., Cao, Q., Chen, J., Chong, A. & Zhan, Q. Toroidal vortices of light. *Nat. Photonics* **16**, 519–522 (2022).
17. Hancock, S., Zahedpour, S. & Milchberg, H. Mode structure and orbital angular momentum of spatiotemporal optical vortex pulses. *Phys. Rev. Lett.* **127**, 193901 (2021).
18. Rego, L. et al. Generation of extreme-ultraviolet beams with time-varying orbital angular momentum. *Science* **364**, eaaw9486 (2019).
19. Malomed, B. A., Mihalache, D., Wise, F. & Torner, L. Spatiotemporal optical solitons. *J. Opt. B: Quantum Semiclassical Opt.* **7**, R53 (2005).
20. Tonomura, A. et al. Observation of individual vortices trapped along columnar defects in high-temperature superconductors. *Nature* **412**, 620–622 (2001).
21. Nagaosa, N. & Tokura, Y. Topological properties and dynamics of magnetic skyrmions. *Nat. Nanotechnol.* **8**, 899–911 (2013).
22. Van Kruining, K., Hayrapetyan, A. G. & Götte, J. B. Nonuniform currents and spins of relativistic electron vortices in a magnetic field. *Phys. Rev. Lett.* **119**, 030401 (2017).
23. Bliokh, K. Y. et al. Theory and applications of free-electron vortex states. *Phys. Rep.* **690**, 1–70 (2017).
24. Schulze, C. et al. Accelerated rotation with orbital angular momentum modes. *Phys. Rev. A* **91**, 043821 (2015).
25. de Oliveira, M. & Ambrosio, A. Subcycle modulation of light's orbital angular momentum via a Fourier space-time transformation. *Sci. Adv.* **11**, eadr6678 (2025).
26. Gui, G., Brooks, N. J., Kapteyn, H. C., Murnane, M. M. & Liao, C.-T. Second-harmonic generation and the conservation of spatio-temporal orbital angular momentum of light. *Nat. Photonics* **15**, 608–613 (2021).
27. Cao, Q., Chen, Z., Zhang, C., Chong, A. & Zhan, Q. Propagation of transverse photonic orbital angular momentum through few-mode fiber. *Adv. Photonics* **5**, 036002–036002 (2023).
28. Lewenstein, M. et al. Generation of optical schrödinger cat states in intense laser–matter interactions. *Nat. Phys.* **17**, 1104–1108 (2021).
29. Lu, L., Joannopoulos, J. D. & Soljačić, M. Topological photonics. *Nat. Photonics* **8**, 821–829 (2014).
30. Khanikaev, A. B. & Alù, A. Topological photonics: robustness and beyond. *Nat. Commun.* **15**, 931 (2024).
31. Barreiro, J. T., Langford, N. K., Peters, N. A. & Kwiat, P. G. Generation of hyperentangled photon pairs. *Phys. Rev. Lett.* **95**, 260501 (2005).
32. Erhard, M., Krenn, M. & Zeilinger, A. Advances in high-dimensional quantum entanglement. *Nat. Rev. Phys.* **2**, 365–381 (2020).
33. Wang, J. et al. Multidimensional quantum entanglement with large-scale integrated optics. *Science* **360**, 285–291 (2018).

Acknowledgements

This work was supported by National Key Research and Development Program of China (Grant No. 2025YFF0515101, [Q.Z.]), National Natural Science Foundation of China (12374318 [G.F.], 12434012 [Q.Z.], 62535013 [Q.Z.], 62365017 [Y.T.]), Science and Technology Commission of Shanghai Municipality (24JD1402600 [Q.Z.]), Key Project of Westlake Institute for Optoelectronics (Grant No. 2023GD007 [Q.Z.].), Yunnan Provincial Major Science and Technology Special Project (Grants No. 202503AP140044 and 202502AS080003 [Y.T.].), Key Project of Yunnan Provincial Basic Research Fund (Grant No. 202401AS070038 [Y.T.].).

Author contributions

D.W.L. and G.Y.F. conceived the original idea and initiated the project. D.W.L. designed and performed the experiments. X.Y.Z. developed the theoretical model and performed the theoretical analysis. Y.H.T., G.Y.F. and Q.W.Z. contributed to the theoretical interpretation. D.W.L. and X.Y.Z. analysed the data. D.J.L., H.M.W., Z.R.T., D.J.S., Z.S.T., X.S.Z. and Z.G.P. contributed to manuscript improvement and discussion. D.W.L., X.Y.Z., G.Y.F. and Q.W.Z. wrote the manuscript with input from all authors. All authors discussed the results and commented on the manuscript.

Competing interests

The authors declare no competing interests.

Additional information

Supplementary information The online version contains supplementary material available at https://doi.org/10.1038/s41467-026-74644-2.

Correspondence and requests for materials should be addressed to Guangyu Fan.

Peer review information *Nature Communications* thanks the anonymous reviewers for their contribution to the peer review of this work. A peer review file is available.